A cyclin-dependent kinase 5-derived peptide inhibits Cdk5/p25 activity and improves neurodegenerative phenotypes

Jinsoo Seo[1,4,6], Ping-Chieh Pao[1,2,6], Oleg Kritskiy[1,2,6], Audrey Lee[1,2], Debasis Patnaik[5], L. Ashely Watson[1,2], Michael Bula[1,2], Scarlett J. Barker[1,2], Jay Penney[1,2], M. Catarina Silva[5], Stephen J. Haggarty[5] and Li-Huei Tsai[1,2,3]

[1] Picower Institute for Learning and Memory, Massachusetts Institute of Technology, Cambridge, MA 02139, USA.

[2] Department of Brain and Cognitive Sciences, Massachusetts Institute of Technology, Cambridge, MA 02139, USA.

[3] Broad Institute of Harvard and Massachusetts Institute of Technology, Cambridge, MA 02142, USA.

[4] Department of Brain and Cognitive Sciences, Daegu Gyeongbuk Institute for Science and Technology, Daegu, 42988, South Korea.

[5] Chemical Neurobiology Laboratory, Center for Genomic Medicine, Departments of Neurology and Psychiatry, Massachusetts General Hospital and Harvard Medical School, Boston, MA 02114, USA.

[6] These authors contributed equally to this work.

Correspondence should be addressed to Li-Huei Tsai (lhtsai@mit.edu)

Conflict of interest

S.J.H. is a member of the scientific advisory board of Psy Therapeutics, Frequency Therapeutics, and Vesigen Therapeutics, none of whom were involved in the present study. L.-H. T. and S.J.H. are also co-founders and members of Scientific Advisory Board of Souvien Therapeutics. L.-H. T., S.J.H. and J.S. have licensed intellectual property related to Cdk5 inhibitory peptide. The remaining authors declare no competing interests.

Acknowledgements

We thank E. McNamara and M. Taylor for mouse colony maintenance and members of Tsai lab for discussion and valuable comments on manuscript. We also thank Harvard's Center for Macromolecular Interactions for access to instrumentation for Biolayer Interferometry (BLI) and Microscale Thermophoresis. S.J.H. received funding from the Tau Consortium, Stuart & Suzanne Steele MGH Research Scholars Program, and Souvien Therapeutics. This work was supported by NIH grants NS051874-22, AG054012, NS102730, and Glenn award for research in biological mechanism of aging to L.-H.T.

Abstract

Aberrant activity of cyclin-dependent kinase (Cdk5) has been implicated in various neurodegenerative diseases. This effect is mediated by pathological cleavage of the Cdk5 activator p35 to produce the truncated product p25, exhibiting increased stability and altered substrate specificity. The benefit of blocking p25 production has been demonstrated in various rodent and human neurodegenerative models. However, important Cdk5/p35 functions in the developing and adult brain have made it challenging to selectively target the detrimental effects of Cdk5/p25 while sparing the physiological functions of Cdk5/p35. Here, we report a 12-amino acid-long peptide fragment derived from Cdk5 (the Cdk5 inhibitory (Cdk5i) peptide) that shows a high binding affinity toward the Cdk5/p25 complex and can efficiently and selectively inhibit Cdk5/p25 kinase activity. Using cellular assays, mouse neurodegeneration models and human cerebral organoids generated from patient-derived iPSCs, we demonstrate beneficial effects of the Cdk5i peptide on various pathological phenotypes including gliosis, DNA damage, and Tau hyperphosphorylation.

66 **Introduction**

67 Unlike other cyclin-dependent kinases (Cdks), Cdk5 is highly expressed in neurons
68 along with its activators p35 and p39. This proline-directed serine/threonine kinase
69 is involved in various signaling pathways in the brain, regulating cortical
70 development, axonal guidance, synaptic plasticity, and learning and memory (Chae et
71 al., 1997; Gilmore et al., 1998; Kim and Ryan, 2010; Seo et al., 2014). The critical
72 importance of Cdk5 for brain development and function was revealed by the studies
73 using transgenic mice lacking its expression; Cdk5 KO mice display lethality at
74 embryonic stages with neuronal migration defects in the cortex and hippocampus
75 among other brain areas (Ohshima et al., 1996; Gilmore et al., 1998). These
76 observations suggested not only a pivotal role for Cdk5 in brain development, but also
77 that its inhibition might cause detrimental effects.

78

79 Dysregulation of Cdk5 activity has been associated with multiple types of brain
80 pathology including neurodegenerative diseases such as Alzheimer's disease and
81 Parkinson's disease (Patrick et al., 1999; Lee et al., 2000; Smith et al., 2003; Seo et al.,
82 2014; Park et al., 2019). One prominent avenue leading to Cdk5 dysregulation is via
83 cleavage of the Cdk5 activator p35 to p25. Various neurodegenerative stimuli,
84 including protein aggregates and oxidative stress can trigger abnormal increases in
85 intracellular calcium levels leading to activation of the calcium-dependent cysteine
86 protease, calpain. Calpain in turn acts on p35, cleaving its N-terminal regulatory motif
87 and generating elevated levels of the p25 proteolytic fragment. p25 maintains the
88 ability to activate Cdk5 but with a longer half-life compared to Cdk5/p35. Calpain-

89 mediated cleavage also removes myristoylated residues that normally tether
90 Cdk5/p35 to membrane sites, liberating Cdk5 and allowing the Cdk5/p25 complex to
91 access additional kinase substrates (Kusakawa et al., 2000; Lee et al., 2000; Su and
92 Tsai, 2011).
93
94 Lack of auto-inhibition and distinct subcellular localization of Cdk5/p25 compared to
95 Cdk5/p35 suggest the need for a tailored approach to specifically target Cdk5/p25
96 for Cdk5-mediated pathology. However, because p25 is a derivative of p35, it is
97 challenging to design inhibitors targeting Cdk5/p25 without affecting Cdk5/p35.
98 Genetic manipulation to generate mutant p35 that is non-cleavable by calpain but still
99 functional (Δp35) has demonstrated the efficacy of blocking p25 activity (Seo et al.,
100 2014). Transgenic mice in which endogenous p35 was replaced with Δp35 were
101 shown to be less susceptible to Alzheimer's disease-related pathology and tauopathy
102 when they were crossed with 5XFAD mice (expressing five familial AD-linked
103 mutations - *APP* KM670/671NL, *APP* I716V, *APP* V717I, *PSEN1* M146L and *PSEN1*
104 L286V) and Tau P301S mice (expressing *MAPT* carrying the P301S mutation) (Seo et
105 al., 2014; 2017). While the Δp35 transgenic model, effectively a p25 knockout, has
106 been critical to understanding the physiological and pathological functions of
107 Cdk5/p25, the translational potential of this approach is very limited. Small
108 molecules such as roscovitine, a kinase inhibitor with specificity for multiple Cdk
109 family members, have also been utilized to study Cdk5 functions. The utility of
110 roscovitine is limited, however, by a lack of specificity for Cdk5 relative to other Cdk
111 family members (including Cdk1, Cdk2, Cdk7 and Cdk9) (Cicenas et al., 2015).

112 An alternative approach has been the design of peptides to inhibit Cdk5/p25 function.
113 Multiple truncated peptides derived from p35, including CIP (Cdk5 inhibitory
114 peptide) and P5, have been tested, in some cases showing inhibition of Cdk5 activity
115 (Zheng et al., 2005; 2010). Among them, the shortest peptide (P5; 24 amino-acids),
116 showed the most effectiveness. A modified form of P5, with C-terminal cell-
117 penetrating transactivator of transcription (TAT) sequences and an N-terminal FITC
118 tag, was further utilized for *in vivo* investigation in several neurodegenerative mouse
119 models. Injection of this modified P5 into 5XFAD mice and CK-p25 mice
120 (overexpressing p25 in forebrain neurons), reduced the hyperactivation of Cdk5 and
121 gliosis, and restored synaptic and cognitive functions (Shukla et al., 2013; 2017).
122
123 Such a peptide-based approach comes with many advantages. As applied in the
124 studies mentioned above, peptides with some modifications can be directly
125 administrated to rodent brains to monitor their actions. Fluorescence polarization
126 assays can likewise be designed to identify small molecule inhibitors mimicking the
127 effects of the peptide in a high-throughput manner (Moerke, 2009; Wei et al., 2015;
128 Hall et al., 2016). It is worth noting that the length of a peptide is the limiting factor in
129 such assays; shorter peptide lengths increased assay efficiency.
130
131 Our earlier efforts determined the structural basis of the Cdk5/p25 interaction
132 (Tarricone et al., 2001) and provided insight for developing a novel inhibitory peptide
133 for Cdk5/p25 derived from the Cdk5 sequence which we report here. This 12-amino-
134 acid long Cdk5 inhibitory peptide (hereafter referred to as 'Cdk5i peptide') has higher

135 binding affinity for Cdk5/p25 than Cdk5 alone or Cdk2, and displays Cdk5/p25-
136 specific inhibitory function without affecting physiological activities of Cdk5 or Cdk2.
137 Importantly, when delivered to mouse models of neurodegenerative disease (Tau
138 P301S and CK-p25 mice), and human cerebral organoids generated from iPSC of
139 patient with frontotemporal dementia (FTD) carrying the *MAPT* P301L mutation, the
140 Cdk5i peptide ameliorated multiple pathological phenotypes associated with
141 neurodegeneration.
142
143
144
145
146
147
148
149
150
151
152
153
154
155
156
157

158 **Materials & Methods**

159 *Cdk5i and scrambled peptides*

160 Cdk5i peptide consists of 12 amino acids (ARAFGIPVRCYS) that is derived from a
161 activation loop (T-loop) of Cdk5 known as the important site for interacting p25
162 (Tarricone et al., 2001). The sequence for the scrambled is AFRSPCARIGYV. For pull-
163 down assay, biotin was tagged at N-terminus of both Cdk5i and scrambled peptides.
164 For intraperitoneal (I.P.) injection to mice and treatment to iPSCs-derived cerebral
165 organoids, the peptides were conjugated with FITC along with a linker (Ahx-GGG) at
166 N-terminus and the TAT-sequence (YGRKKRRQRRR) was tagged at C-terminus. All
167 peptides were synthesized by Peptide 2.0 Inc (Chantilly, VA).

168

169 *Recombinant p25/Cdk5 for Cdk5 kinase activity assays*

170 Recombinant human Cdk5 and p25 with N-terminal GST-tags were expressed by Sf9
171 insect cells via a baculovirus expression system followed by GST affinity purification
172 (BPS Bioscience, San Diego CA).

173

174 *Microscale thermophoresis-based biophysical assays*

175 The binding affinity of Cdk5i peptide was determined by microscale thermophoresis
176 (MST) using reagents, consumables, and Monolith NT.115Pico from NanoTemper
177 Technologies (Munich, Germany). The recombinant CDK5/p25 protein prep with a
178 HIS was kindly provided by Dr. Kenneth S. Kosik, UC Santa Barbara. 6X-HIS tagged
179 CDK5 (CDK5-236H), and 6X-HIS tagged Cdk2 (CDK2-655H) were purchased from
180 Creative Biomart (https://www.creativebiomart.net/). The HIS tagged protein

181 samples were labeled with the red fluorescent dye NT647 using the Monolith NT HIS-
182 tag labeling kit RED-tris-NTA. A serial dilution of the small molecule was made at 2X
183 concentration with the MST assay buffer (50 mM Tris pH 7.4, 150 mM NaCl, 10 mM
184 $MgCl_2$ and 0.01% Brij-35) and subsequently mixed with an equal volume of 2X
185 concentration of the labeled fluorescent protein. The labeled protein and the Cdk5i
186 peptide mix were allowed to incubate, before filling the capillaries. MST assays were
187 performed at a final concentration of 10 nM labeled protein, with 20% LED/excitation
188 power and high MST power (60%) using regular capillaries for Monolith NT.115.
189 Premium capillaries were used to perform MST with the labeled CDK5/p25 prep to
190 improve the quality of data. The MST results were evaluated with the NanoTemper's
191 MO Affinity Analysis software to estimate the $K_{d.}$
192
193 *Biolayer interferometry-based biophysical assays*
194 The binding interaction between the Cdk5i peptide with the recombinant Cdk5/p25
195 protein was also investigated via biolayer interferometry (BLI) using the Octet Red
196 384 instrument (ForteBio, Fremont, California) with 1X PBS with 0.01% Brij-35 as
197 the assay buffer. The same recombinant Cdk5/p25 protein used for the MST assays
198 was labeled with biotin using EZ-LinkNHS-PEG4-Biotinylation Kit (Thermo Scientific,
199 Waltham, MA) and excess reagent was removed with a spin desalting column as per
200 the manufacturer's instruction. The biotinylated recombinant Cdk5/p25 protein for
201 BLI was eluted in 1X phosphate buffered saline (PBS). Streptavidin (SA) sensors were
202 utilized to study the biophysical interaction between the Cdk5i peptide and
203 biotinylated Cdk5/p25 via BLI. Before starting the BLI experiment, the streptavidin

204 sensors were soaked by dipping in 200 μl of assay buffer in a 96-well Greiner Bio-One
205 Black flat bottom plate (#655209). BLI analysis was performed in 80 μL volume in
206 Greiner Bio-One 384-well black flat bottom PP plates (#781209, Greiner, Monroe,
207 North Carolina) with an initial baseline step, followed by loading of 250 nM
208 biotinylated Cdk5/p25. The recombinant protein and the sample analyte (n=5) were
209 organized in a 384-well plate as per a plate map recommended for the 8-channel
210 mode kinetic analysis, where the streptavidin sensors step from low to high
211 concentration of the Cdk5i sample analyte. Subsequent steps included a second
212 baseline (120s), association (240s), and dissociation (240s) for the analysis of
213 samples. All the sensors were loaded with the recombinant biotinylated Cdk5/p25
214 protein, and three sensors with the comparable concentration of DMSO in assay
215 buffer was used as the reference (n=3). The results were analyzed with the Data
216 Acquisition HT 11.0 (Fortebio) following reference subtraction (an average of three
217 sensors) with the 1:1 binding model and fitted globally to estimate the equilibrium
218 dissociation constant.
219
220 *Pull-down assay*
221 Recombinant Cdk5/p25 complex or whole brain lysates were incubated with
222 biotinylated Cdk5i or scrambled peptide in binding buffer (50 mM Tris, 150 mM NaCl,
223 0.1% NP-40, pH 7.5) for overnight at 4°C. The following day, Streptavidin-coated
224 beads (GE Life science) were prepared and washed with binding buffer three times.
225 After the final wash, beads were resuspended to produce a 50% slurry by volume,
226 and added to recombinant Cdk5/p25 complex. After rotating the mixture at 4°C for 1

227 hour, samples were centrifuged at 2,500 rpm for 2 min, and the supernatant were
228 saved as 'flow through'. Resuspended beads were subjected for immunoblotting to
229 detect the interaction between the peptides and Cdk5, Cdk2, p25 or p35.
230
231 *IP-linked kinase assay*
232 Recombinant Cdk5/p25 complex or whole mouse brain lysates were incubated with
233 anti-Cdk5 or anti-Cdk2 antibodies for overnight at 4°C and the immunocomplex was
234 prepared as described previously (Seo et al., 2014), and loaded on SDS-PAGE gel and
235 resolved immediately. After running, the gel was carefully dried with plastic wrap and
236 filter paper to avoid wrinkles, and the dry gel was exposed onto a phosphoscreen
237 overnight. The next day, amount of ^{32}P-Histone H1 was measured using a
238 phosphoimager (GE Typhoon). Coomassie staining was performed to confirm that
239 equal amount of proteins was loaded for each group.
240
241 *Animals*
242 All animal experiments were performed with approval from the MIT Committee on
243 Animal Care (CAC). CK-p25 mice were raised on doxycycline containing diet until 2
244 months of age and then switched to normal diet for two weeks along with I.P. injection
245 of Cdk5i or scrambled peptide. Tau P301S (PS19 line) (Yoshiyama et al., 2007), and
246 wild-type mice were obtained from the Jackson Laboratory (Bar Harbor, ME).
247
248 *Primary Neuronal Culture*

249 Primary neurons were generated from the cortical region of timed pregnancy mice
250 (Swiss-Webster) on day E16. Cells were dissociated into a single cell suspension and
251 maintained in Neurobasal Media (Thermo Fisher Scientific) supplemented with L-
252 glutamine (5 mM), penicillin and streptomycin, and B27 neuronal additive. Cells were
253 plated at $2.5x10^6$ cells/10-cm dish, and then transduced with human 4R0N Tau
254 carrying a P301L mutation at 5 days *in vitro* (DIV). Cultured neurons were treated
255 with Cdk5i or scrambled peptide at a concentration of 10 nM for 6 hours on 14 DIV.
256
257 *iPSCs cultures*
258 FTD patient (*MAPT* P301L +/-)-derived iPSC line (Seo et al., 2017) and its isogenic
259 line in which P301L mutation in *MAPT* was corrected by CRISPR/Cas9 genome editing
260 were cultured on irradiated mouse embryonic fibroblasts (MEFs) in DMEM/F12,
261 HEPES media (Gibco) supplemented with 20% knockout serum replacement (KSR)
262 (Gibco), 1X non-essential amino acids (NEAA), 1X GlutaMAX, (Life Technologies) β-
263 fibroblast growth factor (FGF2, PeproTech) and 0.1 mM 2-mercaptoethanol (Sigma-
264 Aldrich). Original approval for human subject work was obtained under a
265 Partners/Massachusetts General Hospital-approved Institutional Review Board
266 Protocol (#2010P001611/MGH).
267
268 *Generation of isogenic control line*
269 A sgRNA for targeting the P301L site in *MAPT* gene (AACATTAAGCATGTCCCGGGAGG)
270 was designed by http://crispr.mit.edu. And both sgRNA and repair template were
271 synthesized by IDT (Integrated DNA Technologies). The CRISPR/Cas9 plasmid

272 (pSpCas9-2A-GFP, PX458) was purchased from Addgene and the sgRNA was cloned
273 into the plasmid and electroporated into iPSCs followed by FACS and colony
274 inspection as described previously (Ran et al., 2013; Seo et al., 2017).
275
276 *Cerebral organoid culture*
277 Cerebral organoids were generated from iPSCs as described previously (Raja et al.,
278 2016; Seo et al., 2017). In brief, embryoid bodies (EBs) were formed by loading
279 12,000 iPSCs per well into 96-well plates pre-coated with Pluronic acid (1%, F-127,
280 Sigma-Aldrich) and maintained in media consists of Glasgow-MEM supplement with
281 20% KSR, 1X sodium pyruvate, 1X NEAA, 0.1 mM 2-mercaptoethanol, 20 μM ROCK
282 inhibitor (Y-27632, Millipore), 5 μM TGFβ-inhibitor (SB431532, Tocris Biosciences),
283 3 μM Wnt-inhibitor (IWRe1, Tocris Biosciences) for 20 days. Cerebral organoids were
284 then transferred to non-adherent petri-dishes and cultured in media consisted of
285 DMEM/F12 supplemented with 1X Chemically Defined Lipid Concentrate and 1X N2-
286 supplement in 40% O_2/5% CO_2 conditions to promote neuroepithelial formation.
287 From day 35, 5 μM heparin (Sigma-Aldrich), 10% FBS and 1% matrigel (Life Sciences)
288 were added to the medium.
289
290 *Immunoblot Analysis*
291 Cultured neurons or homogenized brain lysates were washed once with cold 1 X PBS
292 and lysed in RIPA buffer (150 mM NaCl, 1% IGEPAL, 0.5% sodium deoxycholate, 0.1%
293 SDS, and 50 mM Tris-HCl, pH 8.0, supplemented with protease and phosphatase
294 inhibitors). Supernatant was collected after centrifugation at 12,000 x g for 10 min at

295 4 °C. Samples were loaded in equal amounts of protein onto a 10% polyacrylamide
296 gel. After electrophoresis, proteins were transferred to Immobilon PVDF 0.45 μm
297 membranes (Millipore). Nonspecific binding was blocked by 5% Bovine Serum
298 Albumin in Tris-buffered saline, 0.05% Tween 20. Membranes were incubated with
299 primary antibody for overnight at 4 °C, and secondary antibodies for 1 hour at RT.
300 Band intensity was analyzed using ImageJ software.
301
302 *Immunohistochemistry*
303 Mice were transcardially perfused with 4% paraformaldehyde in PBS under
304 anesthesia (2:1 of ketamine/xylazine), and the brains were sectioned at 40 μm
305 thickness with a Leica VT1000S vibratome (Leica). Cerebral organoids were fixed
306 with 4% paraformaldehyde for overnight, and transferred to 30% sucrose in PBS and
307 kept until they sink. Dehydrated cerebral organoids were cryosectioned at 40 μm
308 thickness. Sections were permeabilized and blocked in PBS containing 0.2% TritonX-
309 100 and 10% normal donkey serum for 1 hour at RT, then incubated with primary
310 antibody at 4°C overnight. Primary antibody was visualized using the appropriate
311 secondary antibody conjugated to Alexa Fluor 488, Alexa Fluor 594, or Alexa Fluor
312 647 (Thermo Fisher Scientific). Nuclei were visualized with Hoechst 33342 (Thermo
313 Fisher Scientific).
314
315 *Microscopy*

316 All images were captured using a Zeiss LSM 710 confocal microscope and the ZEN
317 software, and analyzed using the ImageJ software (National Institutes of Health,
318 https://imagej.nih.gov/ij/, RRID: SCR_003070).
319
320 *Tau seeding activity assay*
321 Whole brain lysates from Tau P301S mice with Cdk5i or scrambled treated and FRET
322 biosensor cell lines described previously were prepared (Seo et al., 2017). For the
323 assay, cells were plated in a 96-well plate at a density of 40,000 cells/well. Brain
324 homogenate samples were transduced into cells 16 hours later plating at 50%
325 confluence, using 1 μL Lipofectamine/well. After 48 hours incubation, cells were
326 harvested and fixed in 4% paraformaldehyde. An LSR II HST-2 flow cytometer was
327 used to measure the FRET signal in each sample.
328
329 *Antibodies*
330 Cdk5 (C-8, Santa Cruz Biotechnology), p35 (Tsai lab), Cdk2 (SC-163, Santa Cruz
331 Biotechnology), FITC (71-1900, Thermo Fischer Scientific), γ-H2AX (05-636,
332 Millipore), NeuN (266 004, Synaptic Systems), pTau T181 (9632, Cell Signaling
333 Technology), pTau S396 (5383, Cell Signaling Technology), pTau S404 (35834, Cell
334 Signaling Technology), GAPDH (2118, Cell Signaling Technology).
335
336
337
338

339 **Results**

340 Design of Cdk5/p25 complex-specific inhibitory peptide

341 To develop an inhibitory peptide specific to the Cdk5/p25 complex, we utilized our
342 previous work elucidating the crystal structure of the Cdk5/p25 complex, which
343 revealed a critical region in Cdk5 required for the interaction with p25 (Tarricone et
344 al., 2001). This study found by cross-species comparison that the activation loop (T-
345 loop) of Cdk5 is highly conserved from mammals to insects (human, mouse, *Xenopus,*
346 *C. elegans, Drosophila*), but distinct from that of other cyclin-dependent kinases such
347 as Cdk2. We thus selected a 12-amino acid sequence (ARAFGIPVRCYS) from the Cdk5
348 T-loop to generate the Cdk5i peptide (**Figure 1A**). The Cdk5i sequence includes
349 residues R149, A150, I153, C157 and S159, all directed toward the p25 surface and
350 predicted to mediate intermolecular interactions between Cdk5 and p25 (**Figure 1A**).
351

352 To begin to characterize the strength and specificity of Cdk5i peptide binding, we first
353 utilized an *in vitro* binding assay based upon microscale thermophoresis to probe
354 interactions of the peptide with recombinant Cdk5, Cdk2 or Cdk5/p25 complex. We
355 found that the Cdk5i peptide bound to the Cdk5/p25 complex with a K_d = 0.17 μM,
356 which was more than 40-fold more strongly to either Cdk5 or Cdk2 alone (**Figure**
357 **1B**). As an independent biophysical assay, we also verified the binding interaction
358 between the Cdk5i peptide and recombinant Cdk5/p25 protein using biolayer
359 interferometry yielding an affinity measure (K_d = 0.22 μM, **Supplemental Figure 1**).
360 We next utilized pull-down assays using recombinant proteins or brain lysate to
361 probe Cdk5i peptide binding. As a control for peptide sequence specificity, we also

362 included a scrambled peptide (AFRSPCARIGYV) in these experiments. First, the Cdk5i
363 or scrambled peptides were incubated with recombinant Cdk5/p25 complex
364 followed by pull-down. As a bait, the Cdk5i and scrambled peptides were tagged with
365 biotin at their N-terminal and captured by streptavidin-coated beads. We found that
366 the Cdk5i peptide pulled down both Cdk5 and p25 while the scrambled peptide
367 exhibited minimal binding to either protein (**Figure 1C**).
368
369 We then subjected wild-type mouse brain lysates to similar pull-down with the Cdk5i
370 or scrambled peptides to assay their interaction with Cdk5, Cdk2, p25 and p35. We
371 detected no interaction between the scrambled peptide and Cdk5 or Cdk2, while the
372 Cdk5i peptide specifically pulled down Cdk5 but not Cdk2 (**Figure 1D**). p25 and p35
373 can be detected as separate sized bands on western blot with our p35 antibody,
374 however, p25 levels are generally very low under normal physiological conditions.
375 Consistently, we were unable to detect p25 in our brain lysate or following pull-down
376 with the Cdk5i or scrambled peptides (**Figure 1D**). In contrast, we found that p35
377 exhibited interaction with the Cdk5i but not the scrambled peptide under these
378 conditions (**Figure 1D**). Together, these findings show that the Cdk5i peptide binds
379 readily to both recombinant and brain-derived Cdk5 protein and exhibits strong
380 selectivity for Cdk5 over Cdk2.
381
382 <u>Inhibitory action of the Cdk5i peptide on Cdk5/p25 complex function</u>
383 Our *in vitro* binding and pull-down assays demonstrate strong affinity of our Cdk5i
384 peptide for Cdk5 and Cdk5/p25, thus we next wanted to assess whether the Cdk5i

385 peptide exerts an effect on the kinase activity of Cdk5 complexes. We first examined
386 the effect of Cdk5i peptide on kinase activity of the Cdk5/p25 complex prepared from
387 recombinant systems. Compared to Cdk5/p25 complex incubated with scrambled
388 peptide, Cdk5/p25 incubated with Cdk5i peptide showed significantly reduced ability
389 to phosphorylate histone H1, a Cdk substrate (**Figure 2A**).
390
391 To test whether the Cdk5i peptide could likewise exert an inhibitory effect on Cdk5
392 complexes isolated from neurodegenerating mouse brains, we next incubated lysates
393 from Tau P301S mice with Cdk5i or scrambled peptide and performed a Cdk5 kinase
394 assay. We previously reported that inhibition of Cdk5/p25 activity by replacing
395 endogenous p35 with the non-cleavable Δp35 in this mouse model reduced Cdk5
396 activity by about 60% (Seo et al., 2017). Consistently, we found a roughly 50%
397 reduction of Cdk5 activity in P301S mice brain lysates after treatment with the Cdk5i
398 peptide compared to those treated with scrambled peptide (**Figure 2B**).
399
400 To examine whether the Cdk5i peptide can inhibit Cdk5/p35 function, which is
401 known to be critical for neurodevelopment and synaptic function under physiological
402 conditions, we collected brain lysates from wild-type mice. Following incubation of
403 these lysates with either Cdk5i or scrambled peptides, we measured kinase activity
404 for Cdk5. Despite showing physical interaction with p35 from mouse brain (**Figure**
405 **1D**), we found that neither the Cdk5i nor scrambled peptides altered basal Cdk5
406 kinase activity in wild-type brain lysates (**Figure 2C**). Furthermore, Cdk2 activity in
407 wild-type brain lysates was also unaffected by Cdk5i or scrambled peptides (**Figure**

408 **2D**). Thus, the Cdk5i peptide can inhibit the kinase activity of recombinant Cdk5/p25,
409 as well as reducing Cdk5-mediated phosphorylation in Tau P301S but not wild-type
410 brain lysates.
411
412 Preventive effects of the Cdk5i peptide on pathological phenotypes in CK-p25 mice
413 Multiple pathological effects of Cdk5/p25 signaling, as well as the beneficial effects of
414 inhibiting Cdk5/p25 function have been reported in multiple neurodegenerative
415 conditions including Alzheimer's disease and Frontotemporal dementia (FTD)
416 (Shukla et al., 2013; Seo et al., 2014; 2017; Shukla et al., 2017). Thus, we sought to
417 examine the effects of our Cdk5i peptide in neurodegeneration-related phenotypes *in*
418 *vivo*. To that end, we added the TAT sequence (YGRKKRRQRRR) to the C-terminus of
419 the peptide along with conjugating FITC at the N-terminus. The modified version of
420 the peptide was intraperitoneally (IP) injected (40 mg/kg body weight) into CK-p25
421 mice, an inducible model of AD-like neurodegeneration. We were able to detect FITC
422 signal in both hippocampus and cortex 24 hours after a single injection, indicating
423 successful penetration into the brain (**Figure 3A**).
424
425 Two weeks of p25 induction in CK-p25 mice has been shown to be sufficient to induce
426 DNA damage, marking the beginning of a cascade leading to neuronal death (Kim et
427 al., 2008). To test whether Cdk5i peptide treatment could counteract p25-induced
428 DNA damage, we treated CK-p25 mice with the Cdk5i or scrambled peptides three
429 times weekly (IP, 40 mg/kg body weight) during the two-week p25 induction period.
430 Consistent with previous reports, we observed prominent accumulation of DNA

431 damage, marked by immunoreactivity for phosphoserine 139 of histone H2AX
432 (γH2AX), in the CA1 area of hippocampus after two weeks induction (Kim et al., 2008)
433 (**Figure 3B-C**). We found that treatment of CK-p25 mice with the Cdk5i peptide
434 significantly reduced γH2AX signal intensity relative to those receiving the scrambled
435 peptide, though DNA damage remained higher than wild-type mice injected with
436 saline (**Figure 3B-C**).
437
438 Profound gliosis is also an early pathological response to p25 induction, thus we
439 examined astrocyte and microglia changes in the hippocampi of CK-p25 mice by
440 immunohistochemistry with anti-GFAP and anti-IBA1 antibodies, respectively. We
441 found that two-week treatment with the Cdk5i peptide significantly reduced levels of
442 GFAP and IBA1 in the dentate gyrus region and CA3 of the hippocampus relative to
443 scrambled peptide (**Figure 3D-E**). Likewise, the increased size of astrocytes and
444 microglia we observed in the dentate gyrus and CA3 of CK-p25 mice was largely
445 reversed by Cdk5i peptide injection, suggesting attenuation of p25-induced gliosis.
446 Taken together, these data suggest the Cdk5i peptide exerts protective effects on
447 Cdk5/p25-mediated neurodegenerative phenotypes *in vivo*.
448
449 <u>The Cdk5i peptide ameliorates Tau hyperphosphorylation in human and rodent FTD</u>
450 <u>models</u>
451 We next examined the effects of the Cdk5i peptide in tauopathy models which have
452 been strongly associated with Cdk5 hyperactivity (Kimura et al., 2014; Seo et al.,
453 2017). We first overexpressed human 4R0N Tau carrying the FTD-associated P301L

454 mutation in mouse primary neurons starting at DIV 5. Then on DIV 14, we treated
455 cells with either the Cdk5i or scrambled peptide (10 nM) for 6 hours before examining
456 Tau phosphorylation levels by western blotting. Treatment with the Cdk5i peptide
457 induced a significant reduction of Tau phosphorylation on both residues T181 and
458 S396, when compared to treatment with the scrambled peptide (**Figure 4A**).
459
460 We then examined *in vivo* effects of the Cdk5i peptide using the PS19 mouse model of
461 FTD, overexpressing pathogenic human mutant Tau P301S under the control of the
462 prion promoter (Yoshiyama et al., 2007). These mice display increased levels of
463 phosphorylated Tau in brain, and their brain lysates show increased Tau seeding
464 activity when tested using Tau monoclonal FRET biosensor cells (Holmes et al., 2014).
465 We showed previously that these phenotypes were attenuated when p25 generation
466 is abolished in compound PS19; Δp35 transgenic mice (Seo et al., 2017). Either Cdk5i
467 or scrambled peptides were delivered to 3-month-old PS19 mice three times per
468 week by IP injection for one month. We then performed immunostaining to examine
469 levels of pTau. Consistent with data from our *in vitro* experiments with cultured
470 primary neurons (**Figure 4A**), we observed that levels of pTau at multiple residues
471 (T181, S396 and S404) exhibited strong trends toward reduction by Cdk5i peptide
472 treatment compared to mice injected with the scrambled peptide (**Figure 4B**).
473 Hyperphosphorylation of Tau is known to lead to misfolding and aggregation of Tau
474 by liberating the protein from microtubules and exposing its hydrophobic surface
475 (Mazanetz and Fischer, 2007; Kolarova et al., 2012). This insoluble form of Tau is
476 thought to induce propagation of tauopathy across cells by "seeding" the formation of

477 additional aggregates. Therefore, we next utilized FRET biosensor HEK293T cells
478 expressing human Tau carrying P301S mutation and fused with either CFP or YFP to
479 test Tau seeding activity. Compared to scrambled peptide-treated Tau P301S mouse
480 brains, we observed a trend toward reduced seeding effect from Tau P301S brains
481 treated with the Cdk5i peptide (**Figure 4C**).
482
483 We have found striking effects of the Cdk5i peptide treatment in mouse brains and
484 cultured cells. To extend these findings to a human neurodegenerative context, we
485 took advantage of human iPSC models. We utilized iPSCs derived from an FTD patient
486 carrying a heterozygous *MAPT* P301L mutation, and generated isogenic cells where
487 the P301L mutation was corrected by CRISPR/Cas9 genome editing (**Supplementary**
488 **Figure 2**). We previously reported that cerebral organoids derived from the parental
489 *MAPT* P301L line faithfully recapitulate Tau hyperphosphorylation, as observed in
490 patient brains (Seo et al., 2017). Consistently, in cerebral organoids generated from
491 our isogenic pair of iPSC lines, we found increased levels of pTau (pS396 and pS404)
492 in 4-month-old organoids carrying the *MAPT* P301L compared to corrected controls.
493 Importantly, treatment of *MAPT* P301L cerebral organoids for two weeks with the
494 Cdk5i peptide resulted in significantly reduced levels of pTau compared organoids
495 treated with the scrambled peptide (**Figure 4D-F**). Thus, the Cdk5i peptide
496 counteracts pathological Tau hyperphosphorylation in human FTD models as it does
497 in our transgenic mouse and cell-based systems.
498
499

500 **Discussion**

501 We previously showed that genetic modification of p35 to abolish calpain-dependent
502 cleavage and production of p25 successfully attenuated various pathological features
503 associated with AD and FTD in their respective mouse models and cerebral organoids
504 generated from patient-derived iPSCs (Seo et al., 2014; 2017). Non-cleavable mutant
505 p35 (Δp35KI) is a very useful tool to study the role of Cdk5/p25 in various conditions
506 and to elucidate mechanisms of pathogenesis for Cdk5-associated diseases, however,
507 its application as a therapeutic is limited due to the technical and ethical challenges
508 of applying genetic engineering technologies to human patients (Li et al., 2020). Here,
509 we report the generation and initial characterization of a promising alternative
510 treatment option.

511

512 Peptides are highly selective and relatively safe agents for therapeutic intervention.
513 We designed a 12-amino-acid residue peptide based on our previous structural
514 characterization of the Cdk5/p25 complex (Tarricone et al., 2001). We found that this
515 peptide, termed Cdk5i, bound more than 40-fold more strongly to the Cdk5/p25
516 complex in *in vitro* assays than it did to either recombinant Cdk5 or Cdk2, suggesting
517 it is highly specific for Cdk5/p25. Our findings also demonstrated that Cdk5i is
518 capable of inhibiting Cdk5/p25 activity *in vitro* and Cdk5 activity *in vivo.* Importantly,
519 this effect on Cdk5 activity *in vivo* was only observed on Cdk5 complexes isolated
520 from Tau P301S brain lysates but not brain lysates from wild-type mice where
521 Cdk5/p25 levels are expected to be very low. Further, consistent with the weak
522 affinity Cdk5i showed for Cdk2 in our *in vitro* binding assay, we found that Cdk5i had

523 no effect on the kinase activity of Cdk2 isolated from wild-type mouse brains. Thus,
524 Cdk5i appears to show greater specificity for its intended target than existing small
525 molecule inhibitors such as roscovitine, while also being considerably smaller than
526 the peptide inhibitors of Cdk5 previously reported (Cicenas et al., 2015; Zheng et al.,
527 2005; 2010).
528
529 We then explored the *in vivo* effects of Cdk5i by addition of a cell penetrating TAT
530 sequence, as well as a FITC tag to monitor Cdk5i brain penetration and localization.
531 Twenty-four hours after a single IP injection we were able to detect FITC-Cdk5i in
532 both cortical and hippocampal sections, indicating the ability of this peptide to cross
533 the blood-brain barrier to target Cdk5 complexes in the brain. Critically, we also
534 observed striking effects of Cdk5i treatment on multiple early pathological
535 phenotypes in CK-p25 mice, as well as on Tau phosphorylation in FTD-organoids, two
536 neurodegenerative disease models characterized by elevated p25 production and
537 Cdk5/p25 complex activity. Importantly, in addition to ameliorating elevated
538 neuronal DNA damage in CK-p25 mice, Cdk5i treatment also reduced astrogliosis and
539 microgliosis in CK-p25 brains, indicating at least partial reversal of the cascade of
540 cellular changes that envelops all brain cell types during the course of
541 neurodegeneration.
542
543 While we see clear effects of Cdk5i on Cdk5 complex activity and phenotypes *in vitro*
544 and *in vivo*, its precise mode of action remains uncertain. Consisting of a stretch of
545 Cdk5 residues predicted to mediate the interaction with p25, we hypothesized Cdk5i

546 would bind primarily to p25 (and potentially also to p35). We indeed observed highly
547 selective binding of Cdk5i to Cdk5/p25 complexes in our *in vitro* binding assay. We
548 also observed pull-down of p35 by Cdk5i from wild-type mouse brain lysates, but
549 intriguingly also Cdk5 itself, suggesting Cdk5i may bind independently to both Cdk5
550 and its activator proteins. While direct Cdk5i interactions with Cdk5 or its activators
551 may serve to block Cdk5 complex formation, it is important to note that we observed
552 that Cdk5i interacts more than 90-fold more strongly to Cdk5/25 complex than Cdk5
553 alone. Thus, it is possible that complexes containing all of Cdk5, activator and Cdk5i
554 may form with impaired kinase function as opposed to the formation of Cdk5-Cdk5i,
555 p25-Cdk5i or p35-Cdk5i complexes. Additional modes of action for Cdk5i are also
556 conceivable and further experiments will be required to conclusively demonstrate
557 the precise actions of this peptide. Although we saw preventative effects of our
558 modified Cdk5i peptide *in vivo*, it is likely these functions can be improved further by
559 identifying the key residues important for its inhibitory functions and making the
560 peptide even smaller. Furthermore, adding auxiliary sequences may allow for
561 effective delivery to target tissues/organs, increased stability, and prevent unwanted
562 targeting by enzyme modifiers (Kaspar and Reichert, 2013; Fosgerau and Hoffmann,
563 2015).
564
565 The Cdk5i peptide efficiently inhibits Cdk5/p25 activity without affecting basal
566 activity of Cdk5 important for neurodevelopment and physiological function of brain.
567 Therefore, Cdk5i has potential to be applied to not only neurodegenerative diseases
568 such as AD, PD, FTD mentioned earlier, but also various diseases associated with

569 aberrant Cdk5 activity including cancer, stroke and neuropathic pain (Zhang et al.,
570 2012; Meyer et al., 2014; Pozo and Bibb, 2016).
571
572
573
574
575
576
577
578
579
580
581
582
583
584
585
586
587
588
589
590
591

592 **References**

593 Chae T, Kwon YT, Bronson R, Dikkes P, Li E, Tsai LH (1997) Mice lacking p35, a
594 neuronal specific activator of Cdk5, display cortical lamination defects, seizures,
595 and adult lethality. Neuron 18:29–42.

596 Cicenas J, Kalyan K, Sorokinas A, Stankunas E, Levy J, Meskinyte I, Stankevicius V,
597 Kaupinis A, Valius M (2015) Roscovitine in cancer and other diseases. Ann
598 Transl Med 3:135.

599 Fosgerau K, Hoffmann T (2015) Peptide therapeutics: current status and future
600 directions. Drug Discov Today 20:122–128.

601 Gilmore EC, Ohshima T, Goffinet AM, Kulkarni AB, Herrup K (1998) Cyclin-
602 dependent kinase 5-deficient mice demonstrate novel developmental arrest in
603 cerebral cortex. J Neurosci 18:6370–6377.

604 Hall MD, Yasgar A, Peryea T, Braisted JC, Jadhav A, Simeonov A, Coussens NP (2016)
605 Fluorescence polarization assays in high-throughput screening and drug
606 discovery: a review. Methods Appl Fluoresc 4:022001.

607 Holmes BB, Furman JL, Mahan TE, Yamasaki TR, Mirbaha H, Eades WC, Belaygorod
608 L, Cairns NJ, Holtzman DM, Diamond MI (2014) Proteopathic tau seeding
609 predicts tauopathy in vivo. PNAS 111:E4376–E4385.

610 Kaspar AA, Reichert JM (2013) Future directions for peptide therapeutics
611 development. Drug Discov Today 18:807–817.

612 Kim D, Frank CL, Dobbin MM, Tsunemoto RK, Tu W, Peng PL, Guan J-S, Lee B-H, Moy
613 LY, Giusti P, Broodie N, Mazitschek R, Delalle I, Haggarty SJ, Neve RL, Lu Y, Tsai

614 L-H (2008) Deregulation of HDAC1 by p25/Cdk5 in neurotoxicity. Neuron
615 60:803–817.
616 Kim SH, Ryan TA (2010) CDK5 serves as a major control point in neurotransmitter
617 release. Neuron 67:797–809.
618 Kimura T, Ishiguro K, Hisanaga S-I (2014) Physiological and pathological
619 phosphorylation of tau by Cdk5. Front Mol Neurosci 7:65.
620 Kolarova M, García-Sierra F, Bartos A, Ricny J, Ripova D (2012) Structure and
621 pathology of tau protein in Alzheimer disease. Int J Alzheimers Dis
622 2012:731526.
623 Kusakawa G, Saito T, Onuki R, Ishiguro K, Kishimoto T, Hisanaga S (2000) Calpain-
624 dependent proteolytic cleavage of the p35 cyclin-dependent kinase 5 activator
625 to p25. J Biol Chem 275:17166–17172.
626 Lee MS, Kwon YT, Li M, Peng J, Friedlander RM, Tsai LH (2000) Neurotoxicity
627 induces cleavage of p35 to p25 by calpain. Nature 405:360–364.
628 Li H, Yang Y, Hong W, Huang M, Wu M, Zhao X (2020) Applications of genome
629 editing technology in the targeted therapy of human diseases: mechanisms,
630 advances and prospects. Signal Transduct Target Ther 5:1–23.
631 Mazanetz MP, Fischer PM (2007) Untangling tau hyperphosphorylation in drug
632 design for neurodegenerative diseases. Nat Rev Drug Discov 6:464–479.
633 Meyer DA, Torres-Altoro MI, Tan Z, Tozzi A, Di Filippo M, DiNapoli V, Plattner F,
634 Kansy JW, Benkovic SA, Huber JD, Miller DB, Greengard P, Calabresi P, Rosen CL,
635 Bibb JA (2014) Ischemic stroke injury is mediated by aberrant Cdk5. J Neurosci
636 34:8259-8267.

637 Moerke NJ (2009) Fluorescence Polarization (FP) Assays for Monitoring Peptide-
638 Protein or Nucleic Acid-Protein Binding. Curr Protoc Chem Biol 1:1–15.
639 Ohshima T, Ward JM, Huh CG, Longenecker G, Veeranna, Pant HC, Brady RO, Martin
640 LJ, Kulkarni AB (1996) Targeted disruption of the cyclin-dependent kinase 5
641 gene results in abnormal corticogenesis, neuronal pathology and perinatal
642 death. Proc Natl Acad Sci USA 93:11173–11178.
643 Park J et al. (2019) Abnormal Mitochondria in a Non-human Primate Model of
644 MPTP-induced Parkinson's Disease: Drp1 and CDK5/p25 Signaling. Exp
645 Neurobiol 28:414–424.
646 Patnaik D, Pao P-C, Zhao W-N, Silva MC, Hylton NK, Chindavong PS, Pan L, Tsai L-H,
647 Haggarty SJ (2020) Exifone is a Potent HDAC1 Activator with Neuroprotective
648 Activity in Human Neuronal Models of Neurodegeneration. bioRxiv
649 2020:2020.2003.2002.973636.
650 Patrick GN, Zukerberg L, Nikolic M, la Monte de S, Dikkes P, Tsai LH (1999)
651 Conversion of p35 to p25 deregulates Cdk5 activity and promotes
652 neurodegeneration. Nature 402:615–622.
653 Pozo K, Bibb JA (2016) The Emerging Role of Cdk5 in Cancer. Trends Cancer 10:606-
654 618.
655 Raja WK, Mungenast AE, Lin Y-T, Ko T, Abdurrob F, Seo J, Tsai L-H (2016) Self-
656 Organizing 3D Human Neural Tissue Derived from Induced Pluripotent Stem
657 Cells Recapitulate Alzheimer's Disease Phenotypes. PLoS ONE 11:e0161969.
658 Ran FA, Hsu PD, Wright J, Agarwala V, Scott DA, Zhang F (2013) Genome engineering
659 using the CRISPR-Cas9 system. Nat Protoc 8:2281–2308.

660 Seo J, Giusti-Rodríguez P, Zhou Y, Rudenko A, Cho S, Ota KT, Park C, Patzke H,
661 Madabhushi R, Pan L, Mungenast AE, Guan J-S, Delalle I, Tsai L-H (2014)
662 Activity-dependent p25 generation regulates synaptic plasticity and Aβ-induced
663 cognitive impairment. Cell 157:486–498.
664 Seo J, Kritskiy O, Watson LA, Barker SJ, Dey D, Raja WK, Lin Y-T, Ko T, Cho S, Penney
665 J, Silva MC, Sheridan SD, Lucente D, Gusella JF, Dickerson BC, Haggarty SJ, Tsai L-
666 H (2017) Inhibition of p25/Cdk5 Attenuates Tauopathy in Mouse and iPSC
667 Models of Frontotemporal Dementia. J Neurosci 37:9917–9924.
668 Shukla V, Seo J, Binukumar BK, Amin ND, Reddy P, Grant P, Kuntz S, Kesavapany S,
669 Steiner J, Mishra SK, Tsai L-H, Pant HC (2017) TFP5, a Peptide Inhibitor of
670 Aberrant and Hyperactive Cdk5/p25, Attenuates Pathological Phenotypes and
671 Restores Synaptic Function in CK-p25Tg Mice. J Alzheimers Dis 56:335–349.
672 Shukla V, Zheng YL, Mishra SK, Amin ND, Steiner J, Grant P, Kesavapany S, Pant HC
673 (2013) A truncated peptide from p35, a Cdk5 activator, prevents Alzheimer's
674 disease phenotypes in model mice. FASEB J 27:174–186.
675 Smith PD, Crocker SJ, Jackson-Lewis V, Jordan-Sciutto KL, Hayley S, Mount MP,
676 O'Hare MJ, Callaghan S, Slack RS, Przedborski S, Anisman H, Park DS (2003)
677 Cyclin-dependent kinase 5 is a mediator of dopaminergic neuron loss in a mouse
678 model of Parkinson's disease. Proc Natl Acad Sci USA 100:13650–13655.
679 Su SC, Tsai L-H (2011) Cyclin-dependent kinases in brain development and disease.
680 Annu Rev Cell Dev Biol 27:465–491.
681 Tarricone C, Dhavan R, Peng J, Areces LB, Tsai LH, Musacchio A (2001) Structure and
682 regulation of the CDK5-p25(nck5a) complex. Mol Cell 8:657–669.

683 Wei S et al. (2015) Active Pin1 is a key target of all-trans retinoic acid in acute
684 promyelocytic leukemia and breast cancer. Nat Med 21:457–466.
685 Yoshiyama Y, Higuchi M, Zhang B, Huang S-M, Iwata N, Saido TC, Maeda J, Suhara T,
686 Trojanowski JQ, Lee VM-Y (2007) Synapse loss and microglial activation precede
687 tangles in a P301S tauopathy mouse model. Neuron 53:337–351.
688 Zhang HH, Zhang XQ, Wang WY, Xue QS, Lu H, Huang JL, Gui T, Yu BW (2012)
689 Increased synaptophysin is involved in inflammation-induced heat hyperalgesia
690 mediated by cyclin-dependent kinase 5 in rats. PLoS ONE 7:e46666
691 Zheng Y-L, Amin ND, Hu Y-F, Rudrabhatla P, Shukla V, Kanungo J, Kesavapany S,
692 Grant P, Albers W, Pant HC (2010) A 24-residue peptide (p5), derived from p35,
693 the Cdk5 neuronal activator, specifically inhibits Cdk5-p25 hyperactivity and tau
694 hyperphosphorylation. J Biol Chem 285:34202–34212.
695 Zheng Y-L, Kesavapany S, Gravell M, Hamilton RS, Schubert M, Amin N, Albers W,
696 Grant P, Pant HC (2005) A Cdk5 inhibitory peptide reduces tau
697 hyperphosphorylation and apoptosis in neurons. EMBO J 24:209–220.
698
699
700
701
702
703
704
705

706 **Figure Legends**

707 **Figure 1. Design of Cdk5/p25 complex-specific inhibitory peptide.**

708 **A**, Strategy for the design of Cdk5/p25 complex-specific inhibitory peptide (Cdk5i
709 peptide). The structure of Cdk5/p25 complex was downloaded from RCSB protein
710 data bank. **B,** Microscale thermophoresis-based biophysical assays assessing binding
711 of Cdk5i peptide to recombinant proteins. **C**, Recombinant Cdk5/p25 complex was
712 incubated with biotin-conjugated Cdk5i or scrambled peptide for overnight at 4°C,
713 and subjected to pull-down assay with streptavidin-coated beads. Interaction
714 between the peptides and Cdk5, or p25 was addressed by immunoblotting. **D,** Brain
715 lysates from wild-type mice were incubated with Cdk5i peptide or scrambled for
716 overnight at 4°C, and subjected to pull-down assay. Interaction between the peptides
717 and Cdk5, Cdk2 or p35 was addressed by immunoblotting.

718

719 **Figure 2. Inhibitory action of Cdk5i peptide on Cdk5/p25 complex.**

720 **A,** Recombinant Cdk5/p25 complex was incubated with Cdk5i peptide or scrambled
721 overnight at 4°C, and subjected to IP-linked Cdk5 kinase assay. The bar graph
722 represents the relative radioactivity of ^{32}P incorporated into histone H1. **B,** Brain
723 lysates from three-month-old Tau P301S mice were incubated with Cdk5i peptide or
724 scrambled overnight at 4°C, and subjected to IP-linked Cdk5 kinase assay. **C-D,** Brain
725 lysates from three-month-old wild-type mice were incubated with Cdk5i peptide or
726 scrambled overnight at 4°C, and subjected to IP-linked kinase assay for Cdk5 or Cdk2.

727

728 **Figure 3. Preventive effects of Cdk5i peptide on pathological phenotypes in CK-**
729 **p25 mice brain.**
730 **A,** FITC-conjugated Cdk5i peptide was injected to three-month-old CK-p25 mice (IP
731 40 mg/kg body weight) and its expression in hippocampus and cortex was examined
732 using an anti-FITC antibody. **B,** Immunostaining for γ-H2AX and NeuN were
733 performed in hippocampal CA1 region of CK-p25 mice treated with Cdk5i peptide or
734 the scrambled during two weeks of p25 overexpression. **C,** Bar graphs represent the
735 population of γ-H2AX$^+$; NeuN$^+$ cells out of total NeuN$^+$ and the number of NeuN$^+$ cells
736 in CA1 of CK-p25 treated with Cdk5i or scrambled peptide. **D,** Immunostaining for
737 GFAP and IBA-1 were performed in hippocampal dentate gyrus region and CA3 of CK-
738 p25 mice treated with Cdk5i peptide or the scrambled during two weeks of p25
739 overexpression **E,** Bar graphs represent the number of GFAP-, Iba-1-positive cells,
740 levels of GFAP, IBA-1, or size of GFAP-, IBA-1-positive cells in dentate gyrus and CA3
741 of CK-p25 mice treated with Cdk5i peptide or the scrambled during two weeks of p25
742 overexpression.
743
744 **Figure 4. The Cdk5i peptide ameliorates Tau hyperphosphorylation in human**
745 **and rodent FTD models.**
746 **A**, Levels of pTau T181, pTau S396, and GAPDH were measured after Cdk5i or
747 scrambled peptide treatment in mouse primary neurons overexpressing human Tau
748 P301L mutation. The bar graphs represent the quantification of relative
749 immunoreactivity for pTau T181 and pTau S396 normalized to the scrambled-treated
750 group. **B**, Levels of pTau T181, pTau S396, pTau S404, and GAPDH were measured in

751 brain lysates from non-transgenic (lanes 1-3) and Tau P301S mice treated with either
752 scrambled (lanes 4-6) or Cdk5i peptide (lanes 7-9). Three animals in each group were
753 analyzed. The bar graphs represent the quantification of relative immunoreactivity
754 for pTau T181, pTau S396 and pTau S404 normalized to the non-transgenic group. **C**,
755 Four-month-old Tau P301S animals that were treated with either scrambled or Cdk5i
756 peptides (40 mg/kg body weight) for one month followed by cortical tissue
757 harvesting, were used for a Tau seeding assay. Cortical lysates (5 μg) were added to
758 biosensor HEK293T cells, and their Tau seeding activity was assessed by measuring
759 FRET signals. Three animals in each group were analyzed. **D**, Representative images
760 of pTau S396 and pTau S404 in 4.5-month-old cerebral organoids generated from
761 *MAPT* P301L +/- iPSCs with scrambled peptide treatment, *MAPT* P301L +/- iPSCs
762 with Cdk5i peptide treatment and isogenic control iPSCs with scrambled peptide
763 treatment. **E-F**, Bar graphs represent the quantification of immunoreactivity for pTau
764 S396 **(E)** and pTau S404 **(F)** normalized to isogenic control organoids with the
765 scrambled peptide treatment. Three organoids and two sections per organoid were
766 analyzed in each group.
767
768 **Supplementary Figure 1.** Demonstration of direct binding of the Cdk5i peptide to
769 biotinylated Cdk5/p25 via biolayer interferometry. Top, the processed data graph
770 with cdk5i as the analyte (n=5) following reference (n=3) subtraction show the
771 summary of the real-time data acquisition in a binding kinetics experiment. After an
772 initial baseline step in the assay buffer, streptavidin biosensors were dipped into
773 solution with the biotinylated Cdk5/p25 for the loading of the protein onto the

774 biosensors. Subsequently, a second baseline was performed, followed by association
775 and dissociation of the analyte (n=5) in solution. A productive binding interaction
776 leads to distinct spectral shift pattern that is represented on the sensorgram as a
777 change in the wavelength (nm shift). The data were fitted globally with the 1:1
778 binding model and a representative plot of Req vs. Cdk5i concentration for the
779 estimation of the equilibrium dissociation constant K_D is shown (bottom). Additional
780 details on the BLI assay with biotinylated Cdk5/p25 were described previously
781 (Patnaik et al., 2020).
782
783 **Supplementary Figure 2.** Schematics of isogenic control line generation from an
784 FTD patient iPSCs carrying the *MAPT* P301L mutation. Sanger sequencing confirms
785 the insertion of a desired repair template into an FTD patient iPSCs.

Figure 1

A

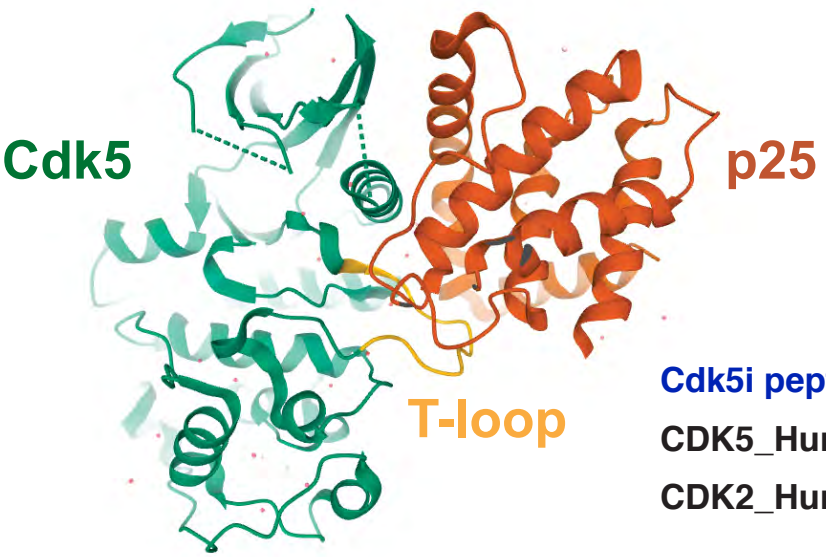

Cdk5i peptide : ARAFGIPVRCYS

CDK5_Human : ...DFGLARAFGI PVRCYSAEVVTL...

CDK2_Human : ...DFGLARAFGVPVRTYTHEVVTL...

B

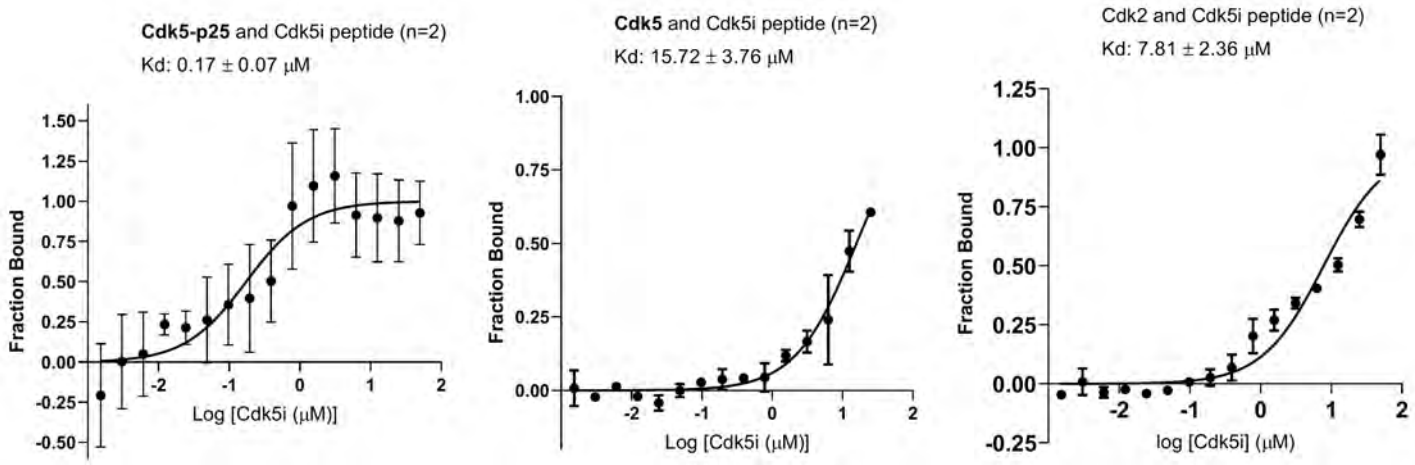

C

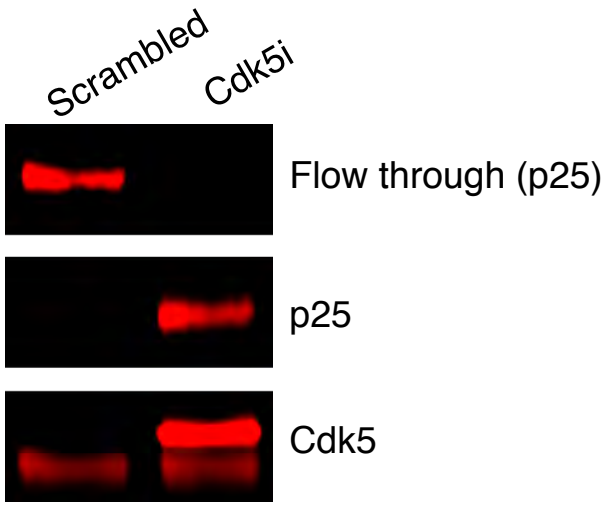

D

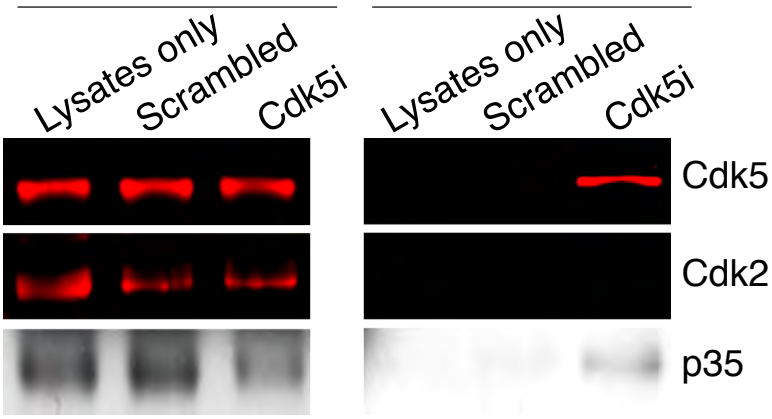

Figure 2

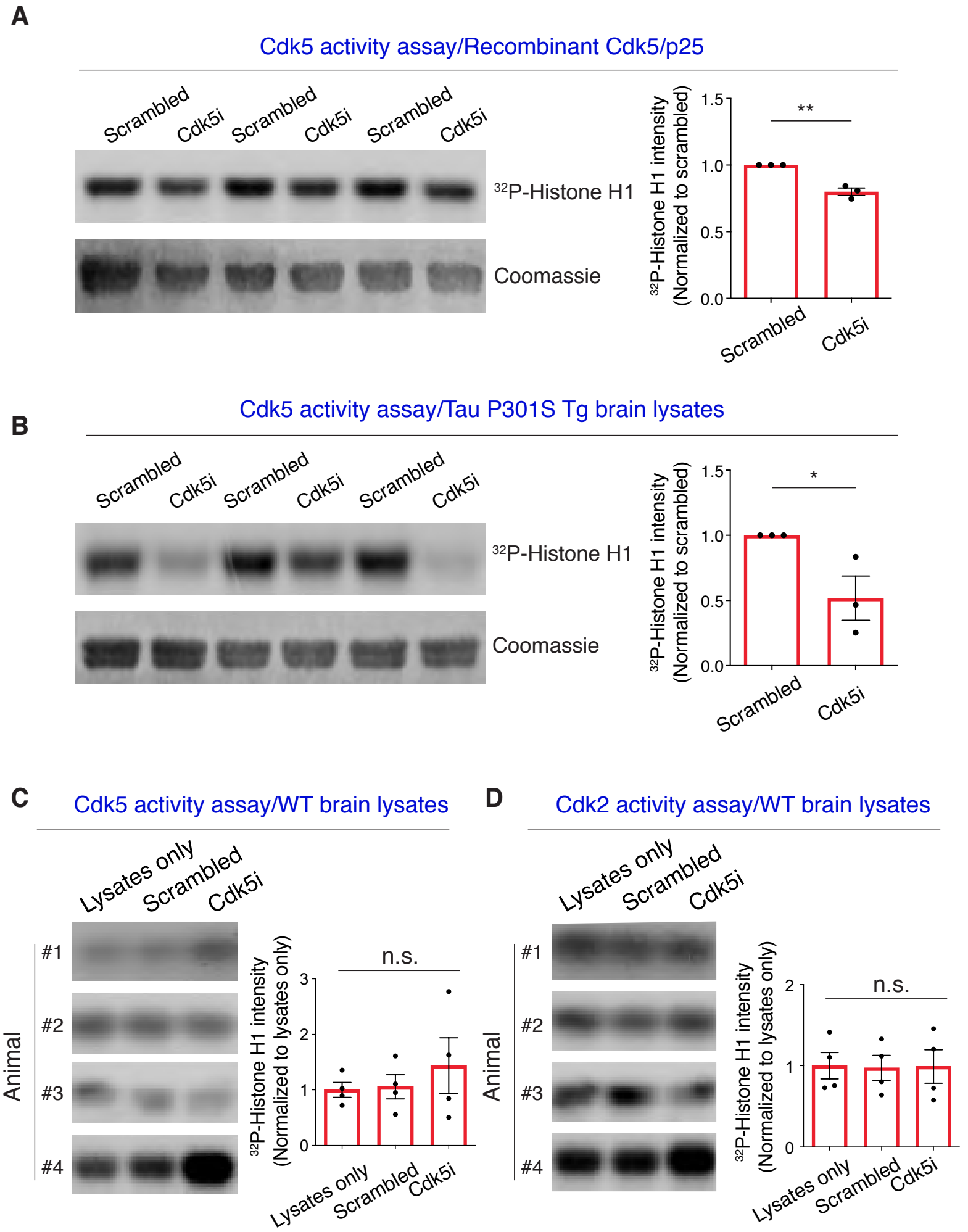
A
Cdk5 activity assay/Recombinant Cdk5/p25
Scrambled
Cdk5i
Scrambled
Cdk5i
Scrambled
Cdk5i
32P-Histone H1
Coomassie
32P-Histone H1 intensity (Normalized to scrambled)
1.5
1.0
0.5
0.0
**
Scrambled
Cdk5i
B
Cdk5 activity assay/Tau P301S Tg brain lysates
Scrambled
Cdk5i
Scrambled
Cdk5i
Scrambled
Cdk5i
32P-Histone H1
Coomassie
32P-Histone H1 intensity (Normalized to scrambled)
1.5
1.0
0.5
0.0
*
Scrambled
Cdk5i
C
Cdk5 activity assay/WT brain lysates
Lysates only
Scrambled
Cdk5i
Animal
#1
#2
#3
#4
32P-Histone H1 intensity (Normalized to lysates only)
3
2
1
0
n.s.
Lysates only
Scrambled
Cdk5i
D
Cdk2 activity assay/WT brain lysates
Lysates only
Scrambled
Cdk5i
Animal
#1
#2
#3
#4
32P-Histone H1 intensity (Normalized to lysates only)
2
1
0
n.s.
Lysates only
Scrambled
Cdk5i

Figure 3

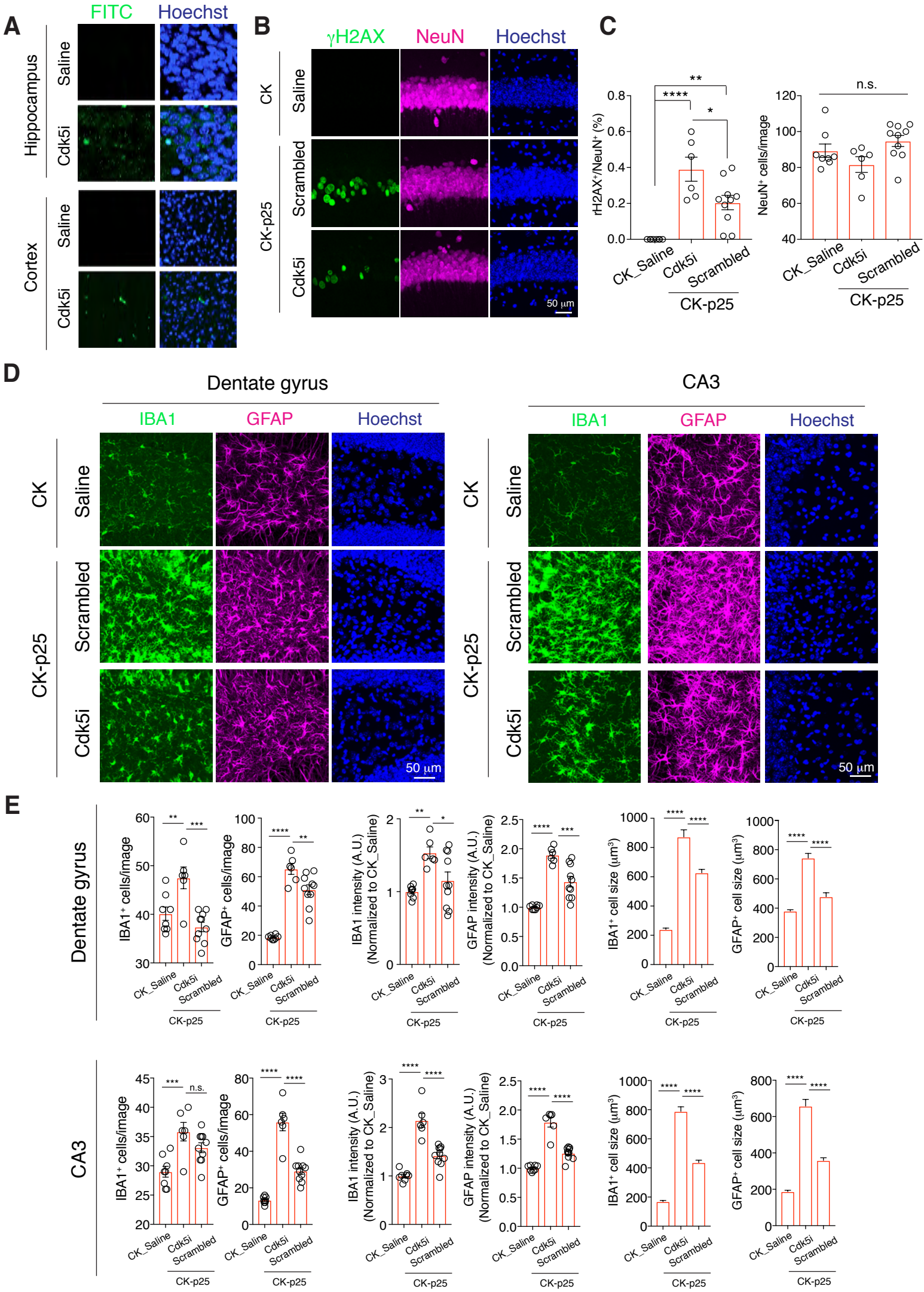
A
FITC
Hoechst
Hippocampus
Saline
Cdk5i
Cortex
Saline
Cdk5i
B
γH2AX
NeuN
Hoechst
CK
Saline
CK-p25
Scrambled
Cdk5i
50 μm
C
rH2AX+/NeuN+ (%)
CK_Saline
Cdk5i
Scrambled
CK-p25
NeuN+ cells/image
n.s.
D
Dentate gyrus
CA3
IBA1
GFAP
Hoechst
CK
Saline
CK-p25
Scrambled
Cdk5i
50 μm
E
Dentate gyrus
CA3
IBA1+ cells/image
GFAP+ cells/image
IBA1 intensity (A.U.) (Normalized to CK_Saline)
GFAP intensity (A.U.) (Normalized to CK_Saline)
IBA1+ cell size (μm3)
GFAP+ cell size (μm3)
CK_Saline
Cdk5i
Scrambled
CK-p25

Figure 4

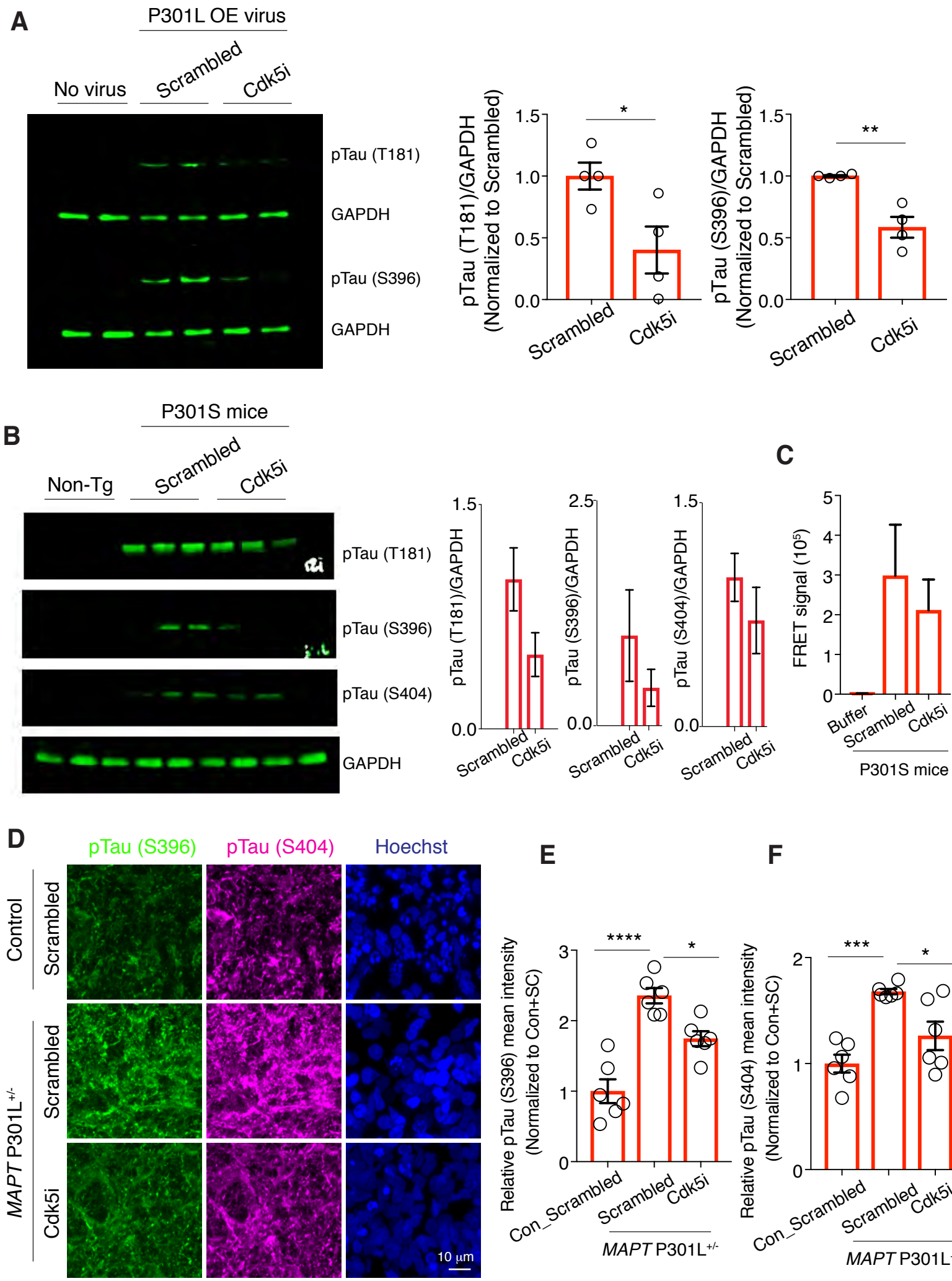
A
P301L OE virus
No virus
Scrambled
Cdk5i
pTau (T181)
GAPDH
pTau (S396)
GAPDH
pTau (T181)/GAPDH (Normalized to Scrambled)
pTau (S396)/GAPDH (Normalized to Scrambled)
B
P301S mice
Non-Tg
Scrambled
Cdk5i
pTau (T181)
pTau (S396)
pTau (S404)
GAPDH
pTau (T181)/GAPDH
pTau (S396)/GAPDH
pTau (S404)/GAPDH
C
FRET signal (10^5)
Buffer
Scrambled
Cdk5i
P301S mice
D
pTau (S396)
pTau (S404)
Hoechst
Control
Scrambled
MAPT P301L+/-
Scrambled
Cdk5i
10 μm
E
Relative pTau (S396) mean intensity (Normalized to Con+SC)
Con_Scrambled
Scrambled
Cdk5i
MAPT P301L+/-
F
Relative pTau (S404) mean intensity (Normalized to Con+SC)
Con_Scrambled
Scrambled
Cdk5i
MAPT P301L+/-

Supplementary Figure 1

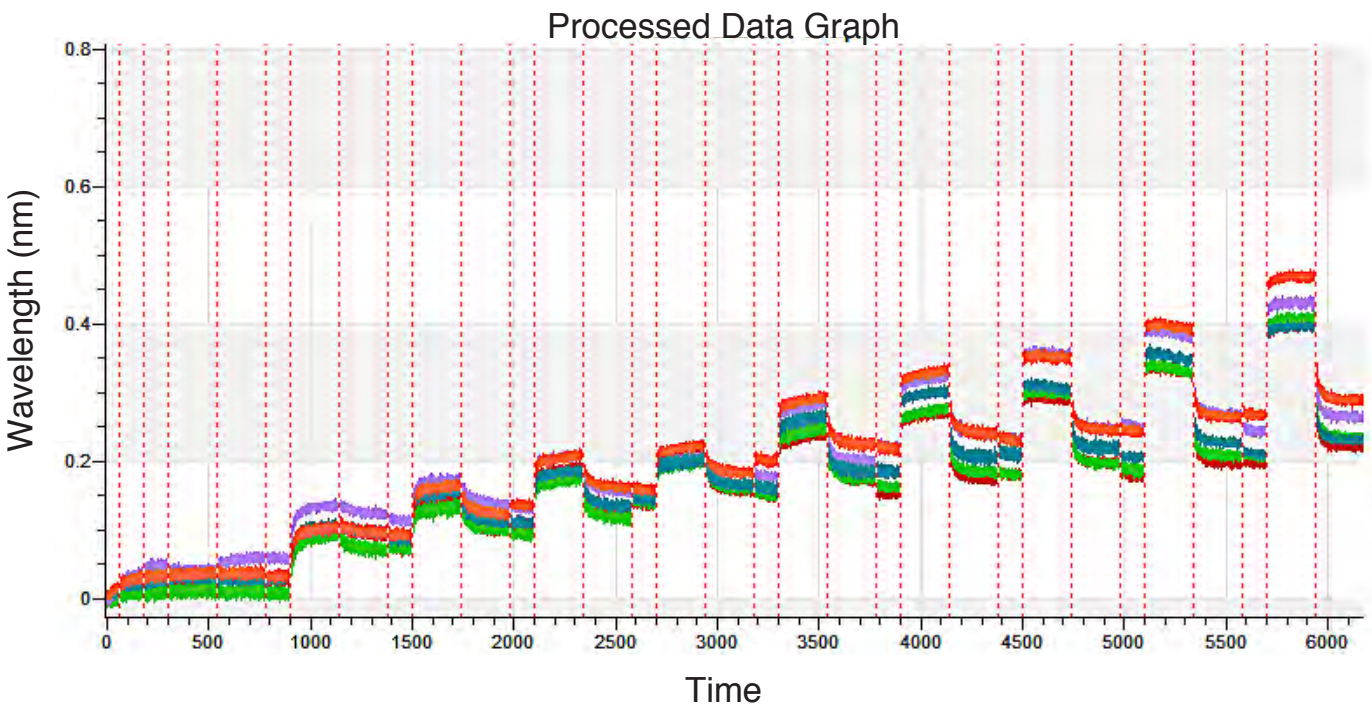

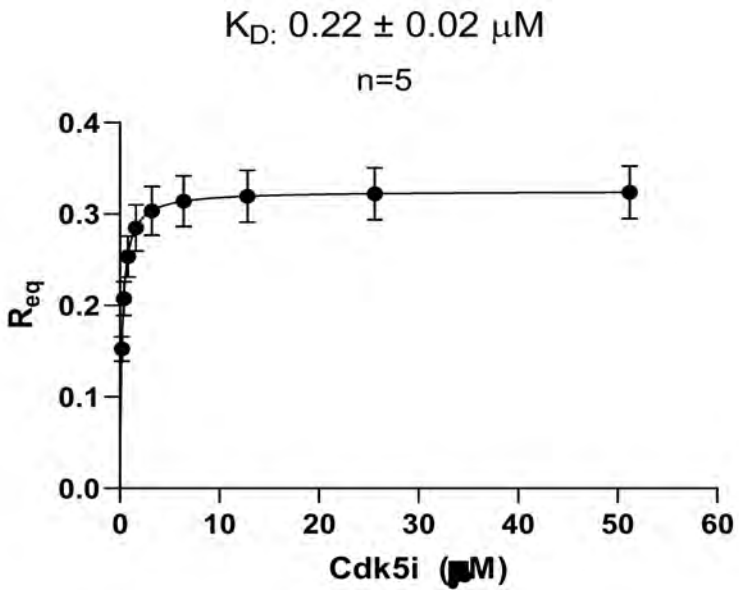
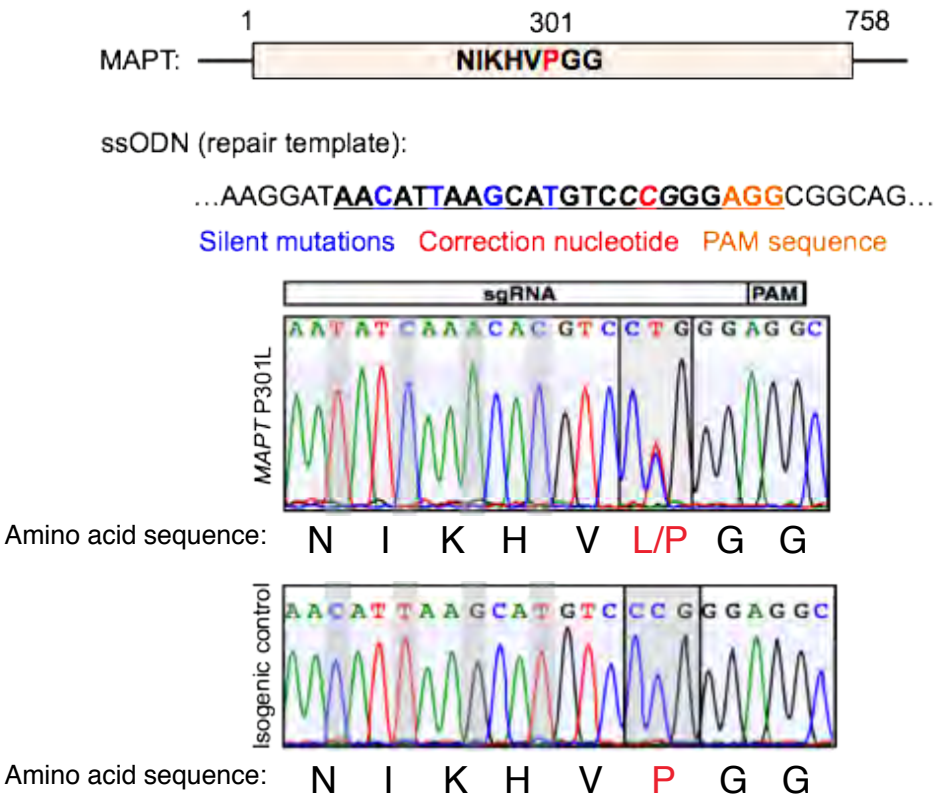
Supplementary Figure 2